# Reactivity of Monolayer Chemical Vapor Deposited Graphene Imperfections Studied Using Scanning Electrochemical Microscopy

**Cen Tan,[†] Joaquín Rodríguez-López,[†] Joshua J. Parks,[†,‡] Nicole L. Ritzert,[†] Daniel C. Ralph,[‡,§] and Héctor D. Abruña[†,*]**

[†]Department of Chemistry and Chemical Biology, [‡]Department of Physics, [§]Kavli Institute at Cornell, Cornell University, Ithaca, New York 14853, United States

**ABSTRACT**

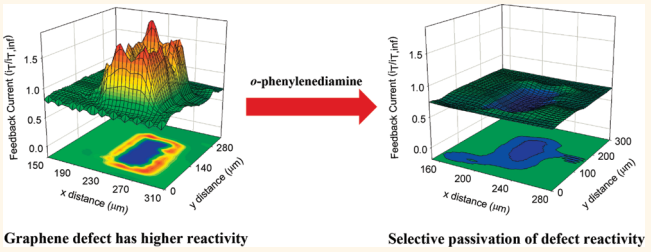


Imperfections that disrupt the $sp^2$ conjugation of graphene can alter its electrical, chemical, and mechanical properties. Here we report on the examination of monolayer chemical vapor deposited graphene imperfections using scanning electrochemical microscopy in the feedback mode. It was found that the sites with a large concentration of defects are approximately 1 order of magnitude more reactive, compared to more pristine graphene surfaces, toward electrochemical reactions. Furthermore, we successfully passivated the activity of graphene defects by carefully controlling the electropolymerization conditions of *o*-phenylenediamine. With further electropolymerization, a thin film of the polymer was formed, and it was found to be insulating in nature toward heterogeneous electron transfer processes. The use of spatially resolved scanning electrochemical microscopy for detecting the presence and the "healing" of defects on graphene provides a strategy for *in situ* characterization and control of this attractive surface, enabling optimization of its properties for application in electronics, sensing, and electrocatalysis.

**KEYWORDS:** graphene · defects · scanning electrochemical microscopy · electrochemistry · *o*-phenylenediamine

Graphene has garnered widespread attention across many scientific disciplines because of its extraordinary electrical, chemical, and mechanical properties. There is increased interest in understanding the chemistry of graphene, controlling its properties through chemical modifications, and using it in applications such as energy storage, sensors, catalysis, and electronics, just to name a few.[1−10] Despite this excitement, many challenges remain in using graphene for practical technologies. For instance, while mechanically exfoliated graphene possesses superb electronic properties,[11] its usefulness in applications is limited because generally only small samples (tens of micrometers wide) can be made. Chemical-vapor deposited (CVD) graphene is more suitable for large-scale processing of graphene,[12] but the fabrication process generally introduces grain boundaries, impurities, and physical damage. These defects can strongly influence the electrical, chemical, and mechanical characteristics of graphene.[13,14] To take full advantage of the properties of graphene in applications, it is necessary to address how defects affect its performance and to develop methods to detect and to control them through means such as passivation.

Graphene defects are generally classified as intrinsic and extrinsic. Intrinsic defects are structural defects, for example, vacancies, carbon adatoms, Stone-Wales defects, and grain boundaries.[13] STM studies have shown an increase in the local density of states at some intrinsic defect sites.[15] Extrinsic defects are the result of the introduction of foreign atoms. Intrinsic defects are prone to attack by foreign atoms to form extrinsic defects due to the strain energy in the carbon−carbon bonds within the structurally unstable intrinsic defects. Computational studies have shown that chemical functional groups can be attached to structural defects.[16,17] For the purpose of the discussions here, all functional groups other than 6-carbon $sp^2$-hybridized structures are treated as defects. Early studies by McCreery and co-workers have shown that surface defects play an important role in the

* Address correspondence to hda1@cornell.edu.

Received for review December 5, 2011 and accepted March 16, 2012.

**Published online March 16, 2012**
**10.1021/nn204746n**

electrochemical activity of highly oriented pyrolytic graphite (HOPG) electrodes.[18−25] On an HOPG surface, a 0.1% increase in defects could result in an increase in the electron charge transfer kinetics of 3 orders of magnitude.[23] These defects are usually composed of phenol, carbonyl, carboxylic acid, lactone, and quinone functional groups.[26] While there have been many computational reports about the reactivity of graphene defects,[27−30] there is a general lack of experimental verification. There have been some examples of electrochemical studies in which the area-averaged characteristics of single layer graphene are modified by oxygenated groups,[31] the insertion of nitrogen,[32] or graphitic islands.[33] Here, we report on spatially resolved measurements of the electrochemical reactivity of graphene and its defects using scanning electrochemical microscopy (SECM). SECM is a powerful tool that can image the surface of a substrate through electrochemical means. It is useful for the determination of heterogeneous electron charge transfer kinetics with spatial resolution and for the fabrication of high-resolution patterns on metal and semiconducting surfaces.[34−37] Studies of the electrochemical activity of carbon nanostructures, where high-accuracy measurement of electron transfer rates was required, have been done using SECM.[38−40]

Defects on graphene can be generated during growth, by ion or electron irradiation, or by chemical oxidation.[13] We introduced defects into our samples by deliberate mechanical damage and by chemical oxidation. The electrochemical reactivity of these graphene defect sites was investigated using the feedback mode of SECM. We examined the passivation of defects on graphene using the electropolymerization of *o*-phenylenediamne (OPD) and studied the mechanism of OPD growth. Electropolymerization of OPD has been widely used in photovoltaic cells, anticorrosion coatings, and biosensors. OPD polymerization has also been used for the selective passivation of imperfections of n-$WSe_2$ and n-$MoSe_2$.[41] The oligomeric structures resulting from OPD electropolymerization have been analyzed previously using mass spectrometry.[42]

## RESULTS AND DISCUSSION

The SECM technique can be employed to measure the heterogeneous electron transfer rate by using what is known, in SECM parlence, as the feedback mode. The use of a bipotentiostat allows the independent control of tip and substrate potentials. In the feedback mode, an SECM tip is held at a potential where a steady state electrochemical reaction of a mediator redox pair *Ox/Red* takes place (Figure 1a). This steady state current, $i_{T,inf}$, resulting from the reduction of *Ox* to *Red*, for instance, is proportional to the number of electrons in the redox process ($n$), Faraday's constant ($F$), the diffusion coefficient of the mediator ($D$), the concentration of the mediator ($C^*_{ox}$), and the radius of the ultramicroelectrode ($r$):

$$i_{T,\,inf} = 4nFDC^*_{Ox}r \qquad (1)$$

As the tip approaches a conductive substrate (Figure 1b), *Red,* generated at the tip, reaches the substrate by diffusion. When the substrate is biased at a potential where it can engage in the reaction opposite to that at the tip, a diffusive feedback loop is established which increases the flux of *Ox* toward the SECM tip. This, in turn, increases the feedback current as a function of decreasing the tip−substrate spacing, $d$ (positive feedback). In contrast, if the tip approaches an insulating substrate (Figure 1c), there is no feedback loop operative. In addition, the current decreases as a function of decreasing $d$ (negative feedback) because diffusion of *Red* to the tip is hindered by the substrate. Figure 1d shows approach curves, which are the current profiles *versus* the normalized distance $L = d/r$, as the tip approaches a conductor (red) and an insulator (blue). The resulting current, also known as the feedback current, provides information about the distance between the working electrodes (tip and substrate) and the rate of heterogeneous electron transfer. Figure 1e shows simulated current profiles for various dimensionless heterogeneous rate constants, $K = kr/D$, where $k$ is the heterogeneous electron transfer rate constant and $D$ is the diffusion coefficient of the mediator. The largest and smallest possible feedback currents at a given distance correspond to complete positive feedback and complete negative feedback, respectively. In our experiments, a Pt ultramicroelectrode was the probe working electrode (tip) and a monolayer CVD graphene electrode was the substrate working electrode.

The choice of mediator is important if one is to detect kinetic differences between pristine and defective areas on the graphene surface. We examined two common mediators, hydroxymethylferrocene (FeMeOH) and potassium ferricyanide [$K_3Fe(CN)_6$]. FeMeOH has a standard potential of $E^0 = 0.21$ V *vs* Ag/AgCl, thus, the Pt tip electrode was held at a potential of $E_T = 0.5$ V *vs* Ag/AgCl to ensure complete diffusion-limited oxidation of the Fe(II) species originally present in solution to Fe(III). The graphene substrate electrode was biased at $E_S = -0.2$ V *vs* Ag/AgCl to ensure complete reduction of the species generated at the tip. Positive feedback was observed when the tip approached the graphene using FeMeOH as mediator (Figure 2a,b). The tip was scanned over the graphene surface at a constant tip−substrate separation of 6 $\mu$m to generate a feedback image of the substrate with an approximate resolution of the radius of the tip (~7.5 $\mu$m). Nanometer-scale topographic features have no influence on the response because these features are 3 orders of magnitude smaller than the distance between the tip and the substrate. Thus, only

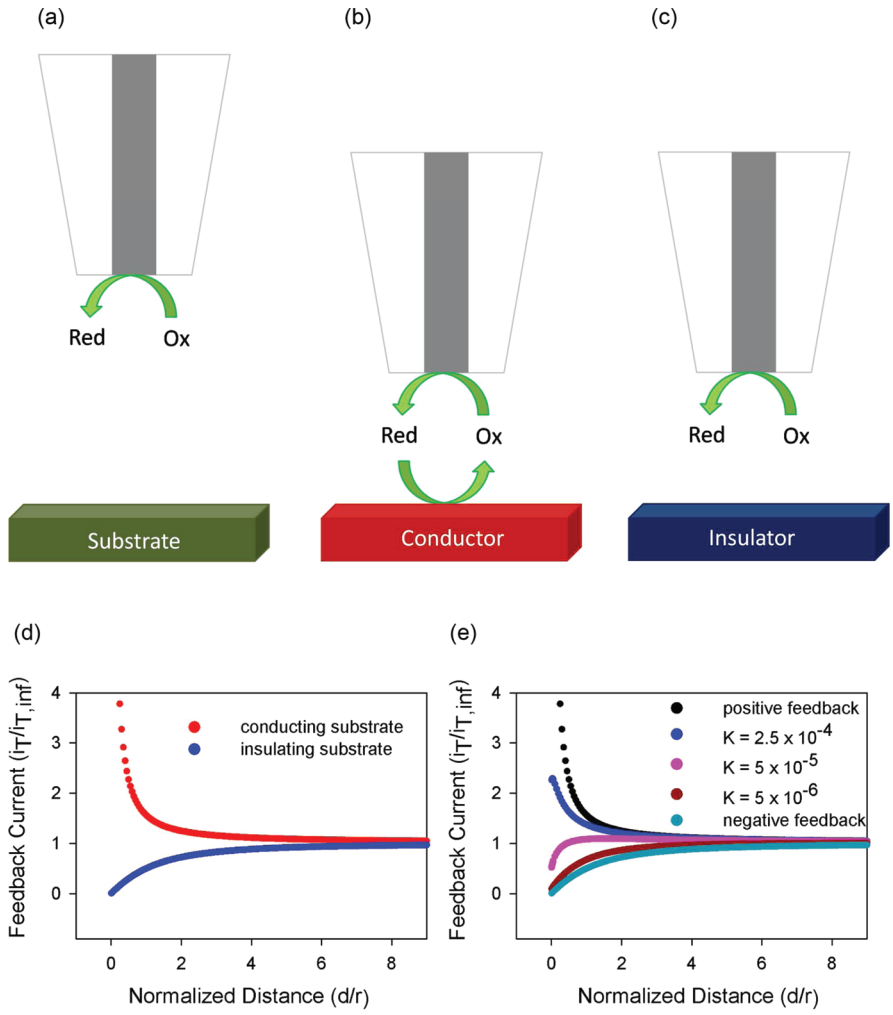


**Figure 1. SECM in the feedback mode: (a) probe electrode far away from substrate electrode, $i_{T,inf}$; (b) probe electrode close to a conducting substrate results in positive feedback current; (c) probe electrode close to an insulating substrate results in negative feedback current; (d) feedback current profiles for conducting and insulating substrates; (e) feedback current profiles varying $K$ ($K = kr/D$) where $r = 7.5$ $\mu$m and $D = 1 \times 10^{-5}$ cm$^2$/s.**

changes in the heterogeneous electron transfer kinetics at the substrate can give rise to changes in the feedback current. The heterogeneous electron transfer rate for FeMeOH at a CVD graphene substrate is very fast, $k_0 = 4.2 \times 10^{-2}$ cm/s, as reported earlier by our group,[43] thus approaching complete positive feedback under conditions described above. In this case, small changes in the kinetics between defects and more pristine areas of graphene cannot be distinguished because of the lack of contrast arising from the fast interfacial kinetics. Occasional voids in the graphene, which exposed the underlying silicon wafer, were created by damaging the graphene surface with a glass tip. This produced insulating areas in the substrate that disabled the feedback loop.

Imaging was also performed using $K_3Fe(CN)_6$ as a mediator, which has a standard potential of $E^0 = 0.16$ V *vs* Ag/AgCl (Figure 2c). $K_3Fe(CN)_6$ has been reported to be highly sensitive to defects on HOPG electrodes with standard heterogeneous rate constants ranging from $8 \times 10^{-7}$ to $4.1 \times 10^{-2}$ cm/s.[22,23] The much slower kinetics, using $K_3Fe(CN)_6$, resulted in intermediate to negative feedback currents (Figure 2d). In our measurements with $K_3Fe(CN)_6$, the tip was held at a potential of $E_T = -0.1$ V *vs* Ag/AgCl to ensure complete reduction of the Fe(III) species originally present in solution to Fe(II), and the graphene electrode was biased at various potentials: $E_S = 0.4$, 0.6, and 0.8 V *vs* Ag/AgCl to regenerate the Fe(III) species. Larger variations (and thus higher contrast) in the electrochemical activity of the graphene surface were observed at all potentials using this mediator compared to FeMeOH which has a much narrower range of heterogeneous kinetics. At 0.8 V *vs* Ag/AgCl, a set of clear, localized defects was observed with size scales ranging up to hundreds of micrometers, providing a strong contrast with respect to a more pristine graphene surface. We propose that different defects may have different chemical or physical identities, leading to a wide range of electron transfer kinetics using $K_3Fe(CN)_6$ as

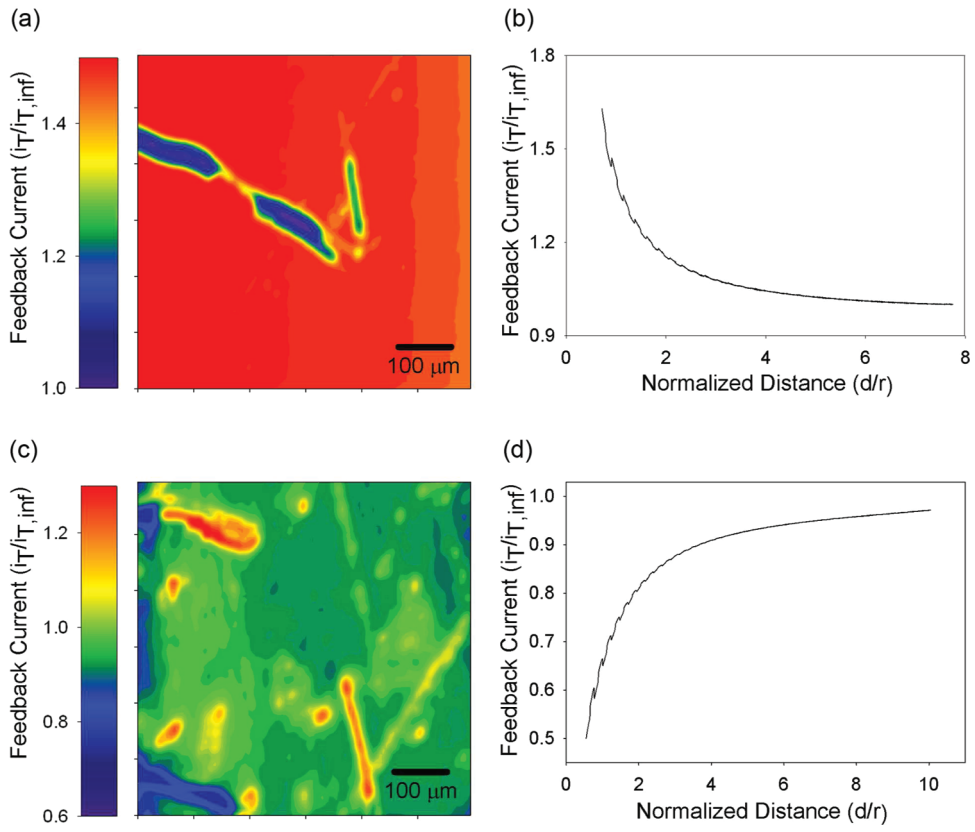


**Figure 2. SECM images of monolayer graphene with different mediators. (a) Positive feedback SECM image showing graphene in red and exposed $Si/SiO_2$ in blue with 1 mM FeMeOH as mediator. The graphene electrode was biased at −0.2 V *vs* Ag/AgCl and the tip was biased at 0.5 V *vs* Ag/AgCl. (b) Positive feedback current profile as the tip approaches a pristine area of the graphene surface. (c) An intermediate-negative feedback SECM image showing the bulk graphene in green/blue and defects of higher activity in orange with 2 mM $K_3Fe(CN)_6$ as the mediator. The graphene electrode was biased at 0.8 V *vs* Ag/AgCl and the tip was biased at −0.1 V *vs* Ag/AgCl. (d) Intermediate-negative feedback current profile as the tip approaches a pristine area of the graphene surface. The large features in the SECM images coincide with regions in which graphene was deliberately removed by scratching the surface with a glass tip.**

mediator. It is important to note that topographic features cannot be observed in this case. Topological features resulting in a smaller $d$ would still give the same negative approach curve followed by a current overload when the tip crashes into these features. This current would be at least a few orders of magnitude higher compared to the usual SECM feedback current. We used $K_3Fe(CN)_6$ as mediator with the graphene electrode biased at $E_S = 0.8$ V *vs* Ag/AgCl because under these conditions, the SECM feedback current depends strongly on the kinetics of the graphene imperfections/defects. In addition, oxidative damage to the graphene surface is unlikely at this potential.

To study the influence of graphene imperfections in a more controlled manner, we created mechanically and chemically induced defects. Optical microscopy images before and after the deliberate creation of defects are available in Figure S1 of the Supporting Information. Mechanical defects were created by damaging the graphene surface with a glass tip using a piezoelectric positioner. Figure 3a shows the schematic of a mechanical defect—a hole in the graphene. The defect and its surrounding areas were examined using SECM as shown in Figure 3b. The edges of the defect show a much higher feedback current than the surface of the graphene far from the defect. The feedback currents correspond to $k_f$ values between $\sim 4.5 \times 10^{-5}$ cm/s for bulk graphene and $\sim 2.6 \times 10^{-4}$ cm/s for defect sites (Supporting Information, Figure S2). This result indicates that the defect sites have higher electron transfer kinetics by approximately an order of magnitude, and thus, are more reactive than the overall surface of graphene. This is in agreement with previous computational and STM results.[15] The higher activities observed on mechanical defects could be due to the exposed edges in the graphene surface and perhaps to the chemical oxidation of $sp^2$ carbons in an aqueous environment. The higher activity of defects on HOPG has been studied thoroughly.[18−25] This result could also explain the higher heterogeneous electron transfer kinetics reported for graphene paste which is smaller in size and therefore high in edge density when compared to the individual monolayer graphene used in this study. Furthermore, it is difficult to distinguish the contributions to the rate of the underlying substrates typically used in the

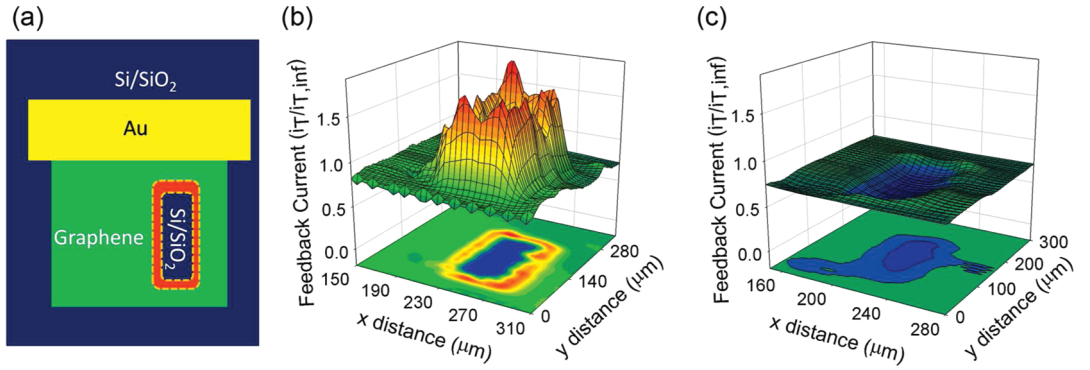


**Figure 3. SECM images of a mechanically induced defect and its passivation: (a) schematic of a mechanically induced defect (not to scale) on the graphene electrode; (b) SECM image of graphene with mechanically induced defect; (c) mechanically induced defect after four cycles of OPD electropolymerization. SECM tip, Pt radius = 7.5 $\mu$m biased at −0.1 V *vs* Ag/AgCl; graphene electrode, biased at 0.8 V *vs* Ag/AgCl; mediator, 2 mM $K_3Fe(CN)_6$; electrolyte, 0.2 M PBS.**

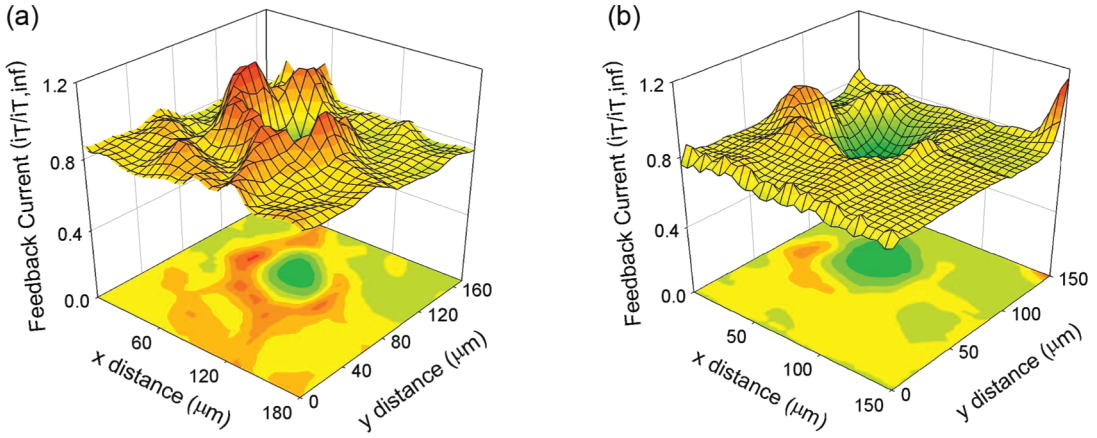


**Figure 4. SECM images of a chemically induced defect and its passivation: (a) chemically induced defect using NaOCl; (b) chemically induced defect after a total of four cycles of OPD electropolymerization. Chemically induced defects were induced by droplets of 10 mM NaOCl. SECM tip, Pt radius = 7.5 $\mu$m biased at −0.1 V *vs* Ag/AgCl; graphene electrode, biased at 0.8 V *vs* Ag/AgCl; mediator, 2 mM $K_3Fe(CN)_6$; electrolyte, 0.2 M PBS.**

graphene paste experiments. In our experiments, the underlying substrate is $Si/SiO_2$ so no such ambiguity is present.

We investigated whether the enhanced electrochemical reactivity of the mechanically induced defects could be passivated by selective electropolymerization of *o*-phenylenediamine (OPD), following the work of Bard and co-workers on the selective passivation of imperfections in n-$WSe_2$ and n-$MoSe_2$ semiconductor electrodes.[41] We immersed the graphene electrode in a solution of OPD and swept its potential between 0 and 0.8 V *vs* Ag/AgCl as shown in Supporting Information, Figure S3. After one cycle of potential sweep, we exchanged the OPD solution with a fresh $K_3Fe(CN)_6$ solution for SECM imaging. A small increase in the feedback current was often observed after the first cycle. This could be due to the competitive desorption of impurities on the graphene that previously could have partially blocked electron transfer or the initial formation of an electrochemically active species on the graphene electrode surface. However, after an additional three potential sweeps, we observed a dramatic decrease in the activity of the active edges, as observed in Figure 3c, indicating that the electrochemically inactive OPD polymer passivated the reactivity of graphene defects. Note, compared to Figure 3b, the overall electrochemical activity of the graphene electrode decreased slightly. This small decrease could be due to either the passivation of widely distributed small defects on the graphene surface by the electropolymerization process or to the electropolymerization of OPD on the pristine surface. Additional experiments suggest the presence of widely distributed defects on graphene, and it is most likely that OPD will attack these defect sites before the pristine areas. The carefully controlled electropolymerization of OPD is able to effectively passivate the active mechanically generated defects while causing little impact on the electrochemical activity of the bulk graphene surface. Upon further electropolymerization of OPD, an insulating film started to form on the graphene surface, diminishing the activity of the entire graphene surface. The possible mechanism of film formation and film thickness will be discussed in a later section.

The reactivity of chemically induced defects was also examined. Arrays of small droplets of an oxidizer,

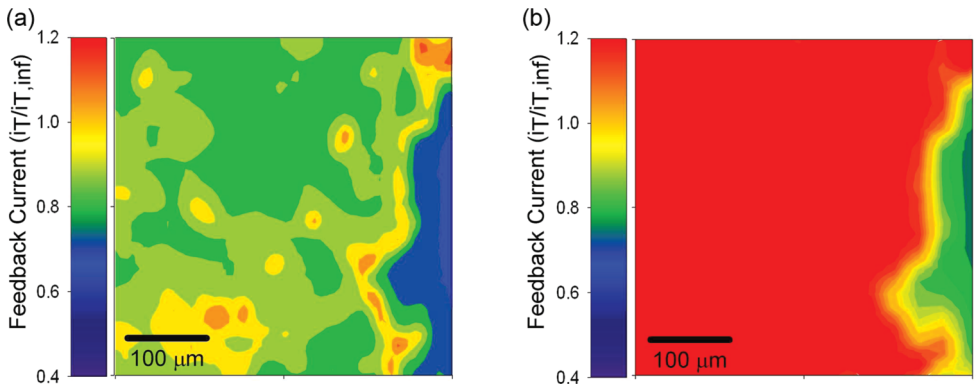


**Figure 5. SECM images of aminoferrocene functionalization experiments on graphene: (a) bare graphene (green, yellow, red) and Si/$SiO_2$ substrate (blue); (b) graphene after aminoferrocene functionalization showing a significant increase in feedback current (red). SECM tip, Pt radius = 7.5 $\mu$m biased at −0.1 V *vs* Ag/AgCl; graphene electrode, biased at 0.8 V *vs* Ag/AgCl; mediator, 2 mM $K_3Fe(CN)_6$; electrolyte, 0.2 M PBS.**

NaOCl, were dispensed onto the graphene electrode using a piezoelectric dispenser. The sample was heated to 100 °C for 30 min to accelerate the oxidative etching process. The graphene was then rinsed with copious amounts of water to remove any remaining NaOCl residues. Small holes of $\sim 30 \times 30\,\mu m^2$ can be observed at the droplet site as shown in Figure 4a. We initially observed a higher feedback current around the edges of the defect and a slight increase in current after one cycle of OPD deposition as seen with the mechanically induced defects. Upon sweeping the potential for an additional three cycles, there was a significant decrease in the activity of the defect sites (Figure 4b). Finally with further cycling, an insulating film of OPD developed. A smaller contrast in activity between the defect sites and the overall graphene, compared to that of mechanical defects, suggests possible differences in the chemical functionalization or defect concentrations. A smaller passivating effect is observed in the chemically induced defect compared to the mechanically induced defects with the same number of polymerization cycles. This discrepancy can be explained by the variation in reactivity toward OPD polymerization of the two types of defects. (We also observe differences between chemically induced and mechanically induced defects in Raman mapping experiments of D band intensity (Supporting Information, Figure S4), similar to previous studies by the groups of Saito and Brus.[44,45]) Despite the possible differences, OPD electropolymerization passivated the defect sites efficiently after a few cycles, while retaining the pre-existing activity of the bulk graphene electrode as was similarly observed in the case of mechanically induced damage

As noted above, while the electropolymerization of OPD successfully passivated the mechanically- and chemically induced defects, a concomitant decrease in the feedback current of the bulk graphene surface was also observed after many cycles. We believe that CVD graphene exhibits many defects and can be passivated by the electropolymerization process, hence the lower feedback current. Because of the instability of structural defects due to strain energies, they are prone to chemical attack by foreign atoms in the environment—most likely oxygen-containing groups. Carboxylic acid functionalized defects are among the most abundant chemical functional groups on carbon materials and can readily react with amino-functionalized groups using an activator such as dicyclohexylcarbodiimide (DCC). As a test, graphene was reacted with an amino-functionalized ferrocene in the presence of DCC. Figure 5 panels a and b show images of a graphene "coastline" (left portion is graphene, right portion is Si/$SiO_2$) before and after the ferrocene functionalization. A comparison of these images shows a dramatic difference in feedback current. The increase in activity is due to the higher electron transfer kinetics of the redox-active ferrocene pendant. The homogeneity indicates that carboxylic acid-functionalized defects exist all over the graphene surface and are functionalized by the ferrocene derivative. This experiment explains why there is a decrease in feedback current over the entire CVD graphene electrode after four cycles of OPD electropolymerization. As shown in Supporting Information, Figure S5, this effect was not observed in the absence of the amino-functionalized ferrocene in the same reaction mixture.

The electropolymerization of *o*-phenylenediamine (OPD) has been previously studied intensively because of its application in electronics and biosensors.[41,46,47] A thin film of OPD started to grow on graphene after sweeping the potential for more than 10 cycles. The formation of this film could possibly serve as a protective or insulating layer in graphene applications, for instance, selective protection of graphene from aggressive solvents and prevention of defect-induced oxidative damage to graphene. To explore the properties of the OPD polymer film, we performed experiments with FeMeOH as the mediator. As mentioned earlier, in a previous study, we had

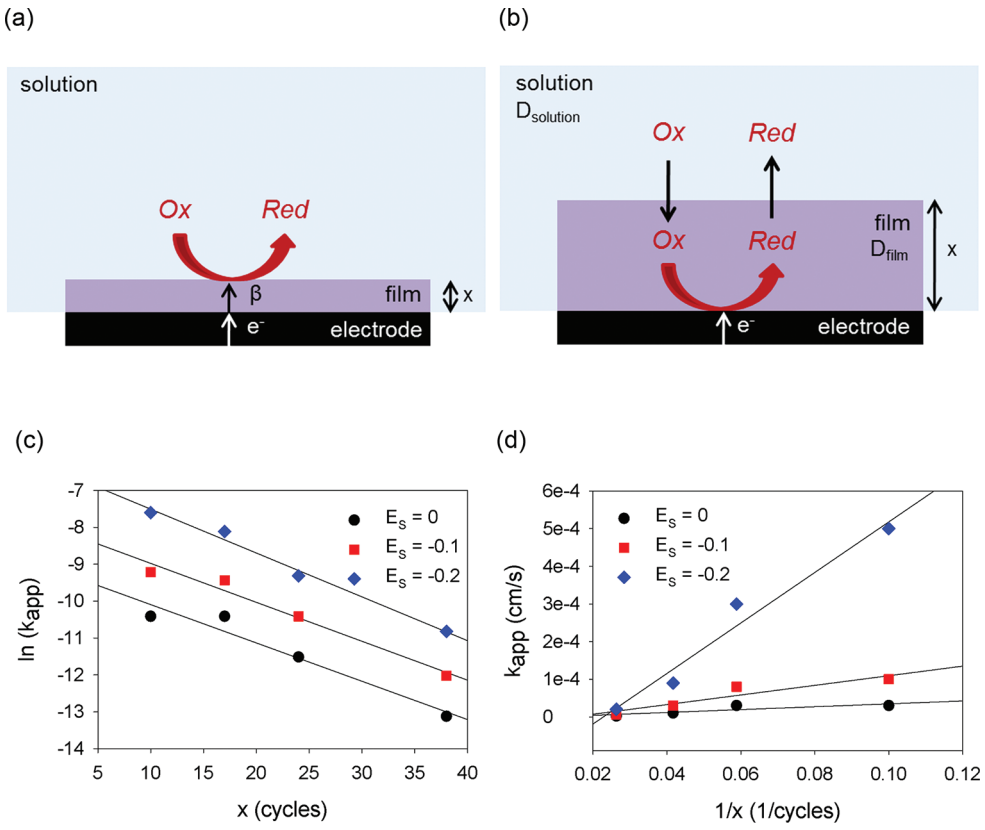


**Figure 6. Determination of the properties of the OPD film on graphene: (a) schematic of electron tunneling through an insulating film; (b) schematic of electron transfer through a permeable film; (c) plot of ln($k_f$) *vs* $x$ following the tunneling model; (d) plot of $k_f$ *vs* 1/$x$ following the permeation model. The unit of $k_{app}$ is cm/s.**

determined the rate constant of FeMeOH at a CVD graphene electrode surface to be $k^0 = 4.2 \times 10^{-2}$ cm/s.[43] FeMeOH is an ideal candidate for probing the barrier properties of the OPD polymer because it shows nearly diffusion limited substrate kinetics—almost complete positive feedback as shown in Figure 2a. At the same time, it has slow enough heterogeneous kinetics that the presence of a thin blocking layer at the electrode would affect the feedback currents in SECM approach curve measurements (Supporting Information, Figure S6).

Two possible electron transfer mechanisms through the OPD film can be proposed and studied using SECM. The first one treats the OPD film as an insulating film for which electron tunneling through the film controls the rate of electrochemical reaction (Figure 6a).[48,49] In this case, the apparent rate of electron transfer can be described by

$$k_{app} = k_f e^{-\beta x} \quad (2)$$

where $k_f$ is the rate of electron transfer of the forward reaction in the absence of the insulating layer, $\beta$ is the tunneling constant which is controlled by the nature of the polymer chain and ranges from 0.4 for $\pi$-conjugated molecules to 1.2 Å$^{-1}$ for saturated chains, and $x$ is the thickness of the film.[50] From the Butler–Volmer formalism, the kinetics of the forward reaction depends on the difference between the substrate potential ($E_S$) and the standard potential ($E^0$),[34] that is, the effective overpotential:

$$k_f = k^0 e^{-\alpha f(E_S - E^0)} \quad (3)$$

where $k^0$ is the standard heterogeneous rate of electron transfer, $\alpha$ is the transfer coefficient, and $f$ = 38.94 V$^{-1}$ at 298 K. Plotting the natural logarithm of $k_{app}$ against $x$ yields a line of slope $\beta$ and a $y$-intercept of $k_f(E)$ where $k_f(E)$ represents the potential-dependent forward rate constant. If evaluated at different substrate potentials, this intercept should show a dependence on $E_S - E^0$, and $k^0$ can be determined by extrapolation. Here we assume that the thickness of the OPD film has a linear dependence on the number of oxidative electropolymerization cycles.

In the second proposed mechanism, the polymer film is permeable.[51−54] Provided that the film is electrochemically inactive and uniform, mediator molecules must partition into the film to complete the redox reaction (Figure 6b). The apparent rate of electron transfer can then be described by

$$k_{app} = \frac{PD_{film}}{x} \quad (4)$$

where the $P$ is the permeability constant, $D_{film}$ is the diffusion coefficient of the mediator in the film, and $x$ is the thickness of the film. In this case, the rate of electron

transfer is inversely dependent on the thickness of the film, regardless of the potential of the substrate electrode.

Figure 6 panels c and d show the plots corresponding to the two scenarios described for rate constants extracted from approach curves obtained at different substrate potentials and different numbers of OPD polymerization cycles. An example of the determination of the rate constants is shown in Supporting Information, Figure S7. A well-correlated linear response was obtained when assuming the electron tunneling mechanism through the blocking layer at a number of oxidative polymerization cycles larger than 10. For less than 10 cycles of OPD polymerization, less than a monolayer is formed. The extrapolated value of $k^0$ in this case is $2 \times 10^{-3}$ cm/s. The strong potential dependence on the measured rates excludes the permeation mechanism, indicating that the tunneling model is more plausible and that the OPD film is insulating. Assuming a $\beta$ value of 0.6 Å$^{-1}$ for $\pi$-conjugated systems, the growth rate of the film on graphene can be extrapolated from the slope to be 20 Å for every 10 cycles.

## CONCLUSIONS

We have examined the spatially resolved electrochemical activity of monolayer CVD graphene imperfections using SECM. $K_3Fe(CN)_6$ was our mediator of choice because it provides good contrast of the electrochemical activity of the defect sites *versus* pristine graphene. The variations in feedback current indicate that the defect sites have very different electron transfer kinetics compared to the overall graphene surface as predicted by computational studies and STM.[15,27−29] By carefully controlling the concentration and the number of oxidative cycles in the electropolymerization of OPD, we selectively passivated the activity of graphene defects. The slight decrease in overall electrochemical activity is believed to be the passivation of inherent defect sites. With further electropolymerization, an insulating thin film of OPD was formed, covering the bulk graphene electrode. We are currently working to improve the spatial resolution of our SECM by fabricating nanosized probe electrodes to examine the defects inherent to the growth and fabrication of graphene.

## METHODS

**Materials.** All chemicals were used as received without further purification unless otherwise stated. The DI water used in these experiments was purified with a Millipore water purification system. Potassium chloride (KCl), sodium sulfate ($Na_2SO_4$), and 0.2 M phosphate buffer (PBS, pH 6.8) were used as electrolyte and were purchased from Mallinckrodt Chemicals. *o*-Phenylenediamine (OPD, 99.5%, Sigma-Aldrich) was recrystallized from ethyl acetate.

**CVD Graphene.** Monolayer graphene was grown by chemical vapor deposition on Cu foil (0.025 mm thick, $1 \times 1$ cm$^2$, 99.8%, Alfa Aesar). The copper foils were treated with acetone (10 s, AR, Mallinckrodt Chemicals), water (DI), glacial acetic acid (10 min, Mallinckrodt Chemicals), water (DI), acetone (10 s), and isopropyl alcohol (10 s, BDH) before growth. They were then loaded into a quartz tube in a tube furnace. The system was pumped to $8.0 \times 10^{-5}$ Torr. After reaching the base pressure, 300 sccm of $H_2$ (99.999%, Airgas) was flowed, and it was present for the entire growth process. The system was then heated at 1000 °C for 10 min, and the graphene was grown under the flow of 157.5 sccm of $CH_4$ (99.999%, Airgas) for 13 min. After removal from the furnace, the graphene was transferred from the Cu foil to an oxidized Si substrate. For support during the transfer, 8% PMMA in anisole (Nano 495 PMMA series resists in anisole, MicroChem) was first spin coated on top of the graphene at 4000 rpm for 60 s. The Cu−graphene−PMMA multilayer was then floated on a ferric chloride etch solution (CE-100 grade, Transene Company) to remove the Cu. The graphene−PMMA membrane was transferred into fresh DI water six times to remove residual impurities. Finally, the membrane was scooped out of DI water with a piece of plasma-cleaned Si/$SiO_2$ substrate (300 nm $SiO_2$, prime grade, Silicon Quest International). The chip was blow-dried using $N_2$ (99.999%, Airgas). To remove the PMMA, the chip was soaked in anisole (2 h, 99.7%, Sigma-Aldrich), dichloromethane (Mallinckrodt Chemicals) and acetone mixture (1:1, 4 h), and isopropyl alcohol (2 h). The quality of the graphene was characterized using a Renishaw InVia Confocal Raman microscope (Renishaw, Gloucestershire, UK) using a 488 nm laser (Supporting Information, Figure S8). The average grain size of the graphene is approximately 0.25−1.7 $\mu$m.[55]

**Electrical Contact to the Graphene.** We used a CVC SC4500 electron-gun evaporator to deposit 20 Å of Ti (99.995%, Kurt J. Lesker Company) onto one end of the single-layer graphene as an adhesion layer followed by 1000 Å of Au (99.999%, Kurt J. Lesker Company).

**SECM Probe Electrode.** The SECM tip was fabricated by inserting a Pt wire (radius $r = 7.5$ $\mu$m, 99.99%, Goodfellow) into a glass capillary tube with a sealed end as reported elsewhere.[35] The capillary tube was heated slowly to melt onto the Pt-wire under vacuum starting from the sealed end. After reaching the desired length, the sealed Pt microwire was exposed and a back contact was made using an InGa eutectic. The tip was sharpened to an RG (thickness of glass/*r*) value of 10, and it was tested electrochemically (steady state voltammetry) to verify its geometric area.

**Electrochemistry.** SECM and electrochemical measurements were carried out using a CHI 900 SECM/potentiostat (CH Instruments, Austin, TX). A homemade Teflon SECM cell was used. A monolayer CVD graphene electrode and a Pt ultramicroelectrode were employed as the substrate and probe electrodes, respectively. Fresh monolayer CVD graphene electrodes were prepared for each experiment. The Pt ultramicroelectrode was polished using 1 $\mu$m alumina on microcloth pads (Buehler) and sonicated in water before each use. A Ag/AgCl saturated KCl reference electrode, isolated from the working electrolyte solution through an agar/0.1 M potassium nitrate bridge to prevent excessive chloride or silver contamination, and a Au wire counter electrode were used. In the mediator selection experiment, 1 mM of hydroxymethylferrocene (FeMeOH, Alfa Aesar) with 0.1 M KCl in water and 2 mM potassium ferricyanide ($K_3Fe(CN)_6$, Fisher Chemicals) in phosphate buffer were employed. Mechanical defects were induced using a glass tip approximately 20 $\mu$m in radius. Chemical defects were created using microdroplets (ranging from 50 to 100 $\mu$m in diameter) of 10 mM NaOCl in water (final pH $\approx$ 8, diluted from a concentrated 5.25% solution, BP) dispensed by a piezoelectric microdispenser with an orifice 30 $\mu$m in diameter (Microfab Inc. Plano, Texas). OPD (13.7 mM) and $Na_2SO_4$ (0.1 M) were prepared in borate buffer (pH 8.1) and the solutions were stored in a dark environment. Electropolymerization of OPD on graphene was carried out by potential cycling between 0 and +0.8 V *vs* Ag/AgCl

at 0.1 V/s for the desired number of cycles. In the carboxylic acid-aminoferrocene coupling reaction, a solution of 2 mM of aminoferrocene (96%, TCI America) and 4 mM of *N*,*N*′-dicyclohexylcarbodiimide (DCC, 99%, Sigma-Aldrich) in *N*,*N*-dimethylformamide (DMF, Mallinckrodt Chemicals) was poured into the electrochemical cell containing the graphene substrate electrode and reacted overnight.

All approach curves and tip positioning procedures were analyzed using reported expressions.[56,57] For feedback imaging experiments, potassium ferricyanide (between 1 and 2 mM) in 0.2 M pH 7 phosphate buffer was used. The SECM tip, $E_T = -0.1$ V *vs* Ag/AgCl, was positioned by a negative feedback-like approach curve obtained with the substrate at open circuit. During imaging, the substrate electrodes were biased to $E_S = 0.8$ V *vs* Ag/AgCl unless noted otherwise. For feedback experiments after deposition of OPD, hydroxymethylferrocene (~1 mM) in 0.1 M potassium chloride was used. The SECM tip, $E_T = 0.4$ V *vs* Ag/AgCl, was positioned by a positive feedback-like approach curve obtained with the substrate at an appropriate potential. In all OPD deposition experiments, care must be taken not to immerse the Pt tip into the deposition solution, as it was observed that even in the absence of tip biasing, the OPD solution would poison the Pt tip so that distorted voltammograms, of otherwise reversible mediators, were observed. For this reason, between each round of OPD deposition and SECM imaging the electrochemical cell was rinsed, at least 10 times, with DI water and the salt bridge was replaced.

*Conflict of Interest:* The authors declare no competing financial interest.

*Acknowledgment.* The work was supported by NSF CCI-phase I (0847926). The authors thank CNF (ECS 0335765) and CCMR (DMR 1120296) for providing fabrication facilities and instrumentations. The authors thank I. Storch, J. Kevek, M. Segal, A. Tsen, Professor P. McEuen, Professor J. Park, and Kevek Innovations for help and providing facilities for graphene growth. C. Tan and N. Ritzert acknowledge NSF IGERT for financial support (DGE 0654193). C. Tan thanks W. Li for useful discussions.

*Supporting Information Available:* Additional information on optical microscopy, $k_f$, electropolymerization, control experiments, and Raman spectroscopy. This material is available free of charge *via* the Internet at http://pubs.acs.org.

## REFERENCES AND NOTES

1. Geim, A. K. Graphene: Status and Prospects. *Science* **2009**, *324*, 1530–1534.
2. Gilje, S.; Han, S.; Wang, M.; Wang, K. L.; Kaner, R. B. A Chemical Route to Graphene for Device Applications. *Nano Lett.* **2007**, *7*, 3394–3398.
3. Yoo, E. J.; Okata, T.; Akita, T.; Kohyama, M.; Nakamura, J.; Honma, I. Enhanced Electrocatalytic Activity of Pt Subnanoclusters on Graphene Nanosheet Surface. *Nano Lett.* **2009**, *9*, 2255–2259.
4. Eda, G.; Chhowalla, M. Graphene-Based Composite Thin Films for Electronics. *Nano Lett.* **2009**, *9*, 814–818.
5. Stoller, M. D.; Park, S.; Zhu, Y.; An, J.; Ruoff, R. S. Graphene-Based Ultracapacitors. *Nano Lett.* **2008**, *8*, 3498–3502.
6. Stankovich, S.; Dikin, D. A.; Dommett, G. H. B.; Kohlhaas, K. M.; Zimney, E. J.; Stach, E. A.; Piner, R. D.; Nguyen, S. T.; Ruoff, R. S. Graphene-Based Composite Materials. *Nature* **2006**, *442*, 282–286.
7. Fowler, J. D.; Allen, M. J.; Tung, V. C.; Yang, Y.; Kaner, R. B.; Weiller, B. H. Practical Chemical Sensors from Chemically Derived Graphene. *ACS Nano* **2009**, *3*, 301–306.
8. Wang, Y.; Shao, Y.; Matson, D. W.; Li, J.; Lin, Y. Nitrogen-Doped Graphene and Its Application in Electrochemical Biosensing. *ACS Nano* **2010**, *4*, 1790–1798.
9. Pumera, M. Electrochemistry of Graphene: New Horizons for Sensing and Energy Storage. *Chem. Rec.* **2009**, *9*, 211–223.
10. Wang, Q. H.; Hersam, M. C. Room-Temperature Molecular-Resolution Characterization of Self-Assembled Organic Monolayers on Epitaxial Graphene. *Nat. Chem.* **2009**, *1*, 206–211.
11. Novoselov, K. S.; Geim, A. K.; Morozov, S. V.; Jiang, D.; Zhang, Y.; Dubonos, S. V.; Grigorieva, I. V.; Firsov, A. A. Electric Field Effect in Atomically Thin Carbon Films. *Science* **2004**, *306*, 666–669.
12. Li, X.; Cai, W.; An, J.; Kim, S.; Nah, J.; Yang, D.; Piner, R.; Velamakanni, A.; Jung, I.; Tutuc, E.; *et al*. Large-Area Synthesis of High-Quality and Uniform Graphene Films on Copper Foils. *Science* **2009**, *324*, 1312–1314.
13. Banhart, F.; Kotakoski, J.; Krasheninnikov, A. V. Structural Defects in Graphene. *ACS Nano* **2010**, *5*, 26–41.
14. Girit, C. O.; Meyer, J. C.; Erni, R.; Rossell, M. D.; Kisielowski, C.; Yang, L.; Park, C.-H.; Crommie, M. F.; Cohen, M. L.; Louie, S. G.; *et al*. Graphene at the Edge: Stability and Dynamics. *Science* **2009**, *323*, 1705–1708.
15. Ugeda, M. M.; Brihuega, I.; Guinea, F.; Gomez-Rodriguez, J. M. Missing Atom as a Source of Carbon Magnetism. *Phys. Rev. Lett.* **2010**, *104*, 096804.
16. Boukhvalov, D. W.; Katsnelson, M. I. Chemical Functionalization of Graphene with Defects. *Nano Lett.* **2008**, *8*, 4373–4379.
17. Cantele, G.; Lee, Y.-S.; Ninno, D.; Marzari, N. Spin Channels in Functionalized Graphene Nanoribbons. *Nano Lett.* **2009**, *9*, 3425–3429.
18. Rice, R. J.; McCreery, R. L. Quantitative Relationship between Electron Transfer Rate and Surface Microstructure of Laser-Modified Graphite Electrodes. *Anal. Chem.* **1989**, *61*, 1637–1641.
19. Rice, R. J.; Pontikos, N. M.; McCreery, R. L. Quantitative Correlations of Heterogeneous Electron-Transfer Kinetics with Surface Properties of Glassy Carbon Electrodes. *J. Am. Chem. Soc.* **1990**, *112*, 4617–4622.
20. Robinson, R. S.; Sternitzke, K.; McDermott, M. T.; McCreery, R. L. Morphology and Electrochemical Effects of Defects on Highly Oriented Pyrolytic Graphite. *J. Electrochem. Soc.* **1991**, *138*, 2412–2418.
21. McDermott, C. A.; Kneten, K.; McCreery, R. L. Electron Transfer Kinetics of Aquated $Fe^{+3/+2}$, $Eu^{+3/+2}$, and $V^{+3/+2}$ at Carbon Electrodes. *J. Electrochem. Soc.* **1993**, *140*, 2593–2599.
22. Kneten, K.; McCreery, R. L. Effects of Redox System Structure on Electron-Transfer Kinetics at Ordered Graphite and Glassy Carbon Electrodes. *Anal. Chem.* **1992**, *64*, 2518–2524.
23. McDermott, M. T.; Kneten, K.; McCreery, R. L. Anthraquinondisulfonate Adsorption, Electron-Transfer Kinetics, and Capacitance on Ordered Graphite Electrodes: The Important Role of Surface Defects. *J. Phys. Chem.* **1992**, *96*, 3124–3130.
24. Cline, K. K.; McDermott, M. T.; McCreery, R. L. Anomalously Slow Electron Transfer at Ordered Graphite Electrodes: Influence of Electronic Factors and Reactive Sites. *J. Phys. Chem.* **1994**, *98*, 5314–5319.
25. McCreery, R. L. Advanced Carbon Electrode Materials for Molecular Electrochemistry. *Chem. Rev.* **2008**, *108*, 2646–2687.
26. Wildgoose, G. G.; Abiman, P.; Compton, R. G. Characterising Chemical Functionality on Carbon Surfaces. *J. Mater. Chem.* **2009**, *19*, 4875–4886.
27. Sanyal, B.; Eriksson, O. Molecular Adsorption in Graphene with Divacancy Defects. *Phys. Rev. B* **2009**, *79*, 113409.
28. Tachikawa, H.; Kawabata, H. Electronic States of Defect Sites of Graphene Model Compounds: A DFT and Direct Molecular Orbital-Molecular Dynamics Study. *J. Phys. Chem. C* **2009**, *113*, 7603–7609.
29. Hu, B. Y.; Hwang, E. H.; Das Sarma, S. Density of States of Disordered Graphene. *Phys. Rev. B* **2008**, *78*, 165411.
30. Ghaderi, N.; Peressi, M. First-Principle Study of Hydroxyl Functional Groups on Pristine, Defected Graphene, and Graphene Epoxide. *J. Phys. Chem. C* **2010**, *114*, 21625–21630.
31. Lim, C. X.; Hoh, H. Y.; Ang, P. K.; Loh, K. P. Direct Voltammetric Detection of DNA and pH Sensing on Epitaxial Graphene: An Insight into the Role of Oxygenated Defects. *Anal. Chem.* **2010**, *82*, 7387–7393.

32. Qu, L.; Liu, Y.; Baek, J.-B.; Dai, L. Nitrogen-Doped Graphene as Efficient Metal-Free Electrocatalyst for Oxygen Reduction in Fuel Cells. *ACS Nano* **2010**, *4*, 1321–1326.
33. Brownson, D. A. C.; Banks, C. E. CVD Graphene Electrochemistry: The Role of Graphitic Islands. *Phys. Chem. Chem. Phys.* **2011**, *13*, 15825–15828.
34. Wipf, D. O.; Bard, A. J. Scanning Electrochemical Microscopy. *J. Electrochem. Soc.* **1991**, *138*, 469–474.
35. Bard, A. J.; Mirkin, M. V. *Scanning Electrochemical Microscopy*; Marcel Dekker: New York, 2001.
36. Bard, A. J.; Fan, F.-R. F.; Mirkin, M. V. In *Electroanalytical Chemistry: Scanning Electrochemical Microscopy*; Bard, A. J., Ed.; Marcel Dekker: New York, 1993; Vol. 18, pp 243–373.
37. Bard, A. J.; Denuault, G.; Lee, C.; Mandler, D.; Wipf, D. O. Scanning Electrochemical Microscopy: A New Technique for the Characterization and Modification of Surfaces. *Acc. Chem. Res.* **1990**, *23*, 357–363.
38. Dumitrescu, I.; Dudin, P. V.; Edgeworth, J. P.; Macpherson, J. V.; Unwin, P. R. Electron Transfer Kinetics at Single-Walled Carbon Nanotube Electrodes using Scanning Electrochemical Microscopy. *J. Phys. Chem. C* **2010**, *114*, 2633–2639.
39. Edwards, M. A.; Bertoncello, P.; Unwin, P. R. Slow Diffusion Reveals the Intrinsic Electrochemical Activity of Basal Plane Highly Oriented Pyrolytic Graphite Electrodes. *J. Phys. Chem. C* **2009**, *113*, 9218–9223.
40. Xie, X.; Zhao, K.; Xu, X.; Zhao, W.; Liu, S.; Zhu, Z.; Li, M.; Shi, Z.; Shao, Y. Study of Heterogeneous Electron Transfer on the Graphene/Self-Assembled Monolayer Modified Gold Electrode by Electrochemical Approaches. *J. Phys. Chem. C* **2010**, *114*, 14243–14250.
41. White, H. S.; Abruna, H. D.; Bard, A. J. Improvement of Performance of n-$WSe_2$ Electrodes by Electrochemical Polymerization of *o*-Phenylenediamine at Surface Imperfections. *J. Electrochem. Soc.* **1982**, *129*, 265–271.
42. Losito, I.; Palmisano, F.; Zambonin, P. G. *o*-Phenylenediamine Electropolymerization by Cyclic Voltammetry Combined with Electrospray Ionization-Ion Trap Mass Spectrometry. *Anal. Chem.* **2003**, *75*, 4988–4995.
43. Li, W.; Tan, C.; Lowe, M. A.; Abruna, H. D.; Ralph, D. C. Electrochemistry of Individual Monolayer Graphene Sheets. *ACS Nano* **2011**, *5*, 2264–2270.
44. Pimenta, M. A.; Dresselhaus, G.; Dresselhaus, M. S.; Cancado, L. G.; Jorio, A.; Saito, R. Studying Disorder in Graphite-Based Systems by Raman Spectroscopy. *Phys. Chem. Chem. Phys.* **2007**, *9*, 1276–1290.
45. Liu, H.; Ryu, S.; Chen, Z.; Steigerwald, M. L.; Nuckolls, C.; Brus, L. E. Photochemical Reactivity of Graphene. *J. Am. Chem. Soc.* **2009**, *131*, 17099–17101.
46. Lowry, J. P.; McAteer, K.; Atrash, S. S. E.; Duff, A.; O'Neill, R. D. Characterization of Glucose Oxidase-Modified Poly-(phenylenediamine)-Coated Electrodes *in Vitro* and *in Vivo*: Homogeneous Interference by Ascorbic Acid in Hydrogen Peroxide Detection. *Anal. Chem.* **1994**, *66*, 1754–1761.
47. Losito, I.; De Giglio, E.; Cioffi, N.; Malitesta, C. Spectroscopic Investigation on Polymer Films Obtained by Oxidation of *o*-Phenylenediamine on Platinum Electrodes at Different pHs. *J. Mater. Chem.* **2001**, *11*, 1812–1817.
48. Liu, B.; Bard, A. J.; Mirkin, M. V.; Creager, S. E. Electron Transfer at Self-Assembled Monolayers Measured by Scanning Electrochemical Microscopy. *J. Am. Chem. Soc.* **2004**, *126*, 1485–1492.
49. Kiani, A.; Alpuche-Aviles, M. A.; Eggers, P. K.; Jones, M.; Gooding, J. J.; Paddon-Row, M. N.; Bard, A. J. Scanning Electrochemical Microscopy. 59. Effect of Defects and Structure on Electron Transfer through Self-Assembled Monolayers. *Langmuir* **2008**, *24*, 2841–2849.
50. Bard, A. J.; Faulkner, L. R. *Electrochemical Methods*, 2nd ed.; John Wiley & Sons: Hoboken, NJ, 2000.
51. Williams, M. E.; Benkstein, K. D.; Abel, C. A.; Dinolfo, P. H.; Hupp, J. T. Shape-Selective Transport through Rectangle-Based Molecular Materials: Thin-Film Scanning Electrochemical Microscopy Studies. *Proc. Natl. Acad. Sci. U.S.A.* **2002**, *99*, 5171–5177.
52. Williams, M. E.; Hupp, J. T. Scanning Electrochemical Microscopy Assessment of Rates of Molecular Transport through Mesoporous Thin-Films of Porphyrinic "Molecular Squares". *J. Phys. Chem. B* **2001**, *105*, 8944–8950.
53. Williams, M. E.; Stevenson, K. J.; Massari, A. M.; Hupp, J. T. Imaging Size-Selective Permeation through Micropatterned Thin Films Using Scanning Electrochemical Microscopy. *Anal. Chem.* **2000**, *72*, 3122–3128.
54. Cornut, R.; Lefrou, C. Studying Permeable Films with Scanning Electrochemical Microscopy (SECM): Quantitative Determination of Permeability Parameter. *J. Electroanal. Chem.* **2008**, *623*, 197–203.
55. Huang, P. Y.; Ruiz-Vargas, C. S.; van der Zande, A. M.; Whitney, W. S.; Levendorf, M. P.; Kevek, J. W.; Garg, S.; Alden, J. S.; Hustedt, C. J.; Zhu, Y.; *et al*. Grains and Grain Boundaries in Single-Layer Graphene Atomic Patchwork Quilts. *Nature* **2011**, *469*, 389–392.
56. Lefrou, C.; Cornut, R. Analytical Expressions for Quantitative Scanning Electrochemical Microscopy (SECM). *ChemPhysChem* **2010**, *11*, 547–556.
57. Bard, A. J.; Mirkin, M. V.; Unwin, P. R.; Wipf, D. O. Scanning Electrochemical Microscopy. 12. Theory and Experiment of the Feedback Mode with Finite Heterogeneous Electron-Transfer Kinetics and Arbitrary Substrate Size. *J. Phys. Chem.* **1992**, *96*, 1861–1868.